



ELSEVIER

Available online at www.sciencedirect.com

SCIENCE @ DIRECT®

New Astronomy 10 (2005) 425–438

New Astronomy

www.elsevier.com/locate/newast

Molecular abundance variations near our galactic center

Y.C. Minh ^{a,*}, S.-J. Kim ^b, Soojong Pak ^a, Sungho Lee ^a,
W.M. Irvine ^{c,d}, L.-Å. Nyman ^e

^a Korea Astronomy and Space Science Institute, 61-1, Hwaam, Yuseong, Daejeon 305-348, Korea

^b Department of Astronomy and Space Science, KyungHee University, Yong-In, Gyunggi-do 449-701, Korea

^c FCRAO, University of Massachusetts, Amherst MA 01003, USA

^d Department of Astronomy, University of Massachusetts, Amherst MA 01003, USA

^e SEST, European Southern Observatory, Casilla, Chile

Received 16 July 2004; received in revised form 25 February 2005; accepted 1 March 2005

Available online 17 March 2005

Communicated by D.B. Sanders

Abstract

Millimeter-wave observations of CO, HCO⁺, HNCO, and SiO molecular lines toward Sgr A show that the prominent gas condensations in this region differ significantly in their chemical properties, which may be a result of gradients in the physical conditions as a function of location. HNCO and SiO observations suggest that $M - 0.13 - 0.08$ (the +20 km s⁻¹ cloud) appears to consist of two different components, $M - 0.13 - 0.08a$ and $M - 0.13 - 0.08b$, with LSR velocities of about +25 and +5 km s⁻¹, respectively. The clump $M - 0.13 - 0.08a$ (the +25 km s⁻¹ cloud) seems to be located very close to Sgr A East and the observed enhancement of HNCO and SiO may result from the interaction with Sgr A East. The molecular gas clump $M - 0.02 - 0.07$ (the +50 km s⁻¹ cloud) shows the strongest ¹³CO emission among the identified clouds in this region, and is the most massive condensation ($\geq 3 \times 10^5 M_{\odot}$), but may be located closer to us than other clouds, since it appears to be chemically quiescent and shade the “inter-cloud region” where the HCO⁺/¹³CO ratio is enhanced. The -30 km s⁻¹ component shows a similar morphology to the HCO⁺ enhanced “inter-cloud” region. $M + 0.07 - 0.08$ and $M + 0.11 - 0.08$ show strong HCO⁺ 1–0 emission, and appear to consist of one cloud (the HCO⁺ cloud) in this observation. The HCO⁺/¹³CO abundance ratio is enhanced by a factor of 2–3 toward this HCO⁺ cloud and the inter-cloud region between $l = 0.1^{\circ}$ and 0° near to Sgr A East, compared to other clouds observed in this region. This relative enhancement of HCO⁺ is thought to result from interaction with Sgr A East.

© 2005 Elsevier B.V. All rights reserved.

PACS: 95.85.Bh

Keywords: Interstellar medium; Sgr A; Gas abundances; Interstellar molecules; CO; HCO⁺; HNCO; SiO molecule

* Corresponding author. Tel.: +82 42 865 3263; fax: +82 42 861 5610.

E-mail addresses: minh@trao.re.kr (Y.C. Minh), sjkim1@khu.ac.kr (S.-J. Kim), soojong@kao.re.kr (S. Pak), leesh@kao.re.kr (S. Lee), irvine@fcrao1.astro.umass.edu (W.M. Irvine), lnyman@eso.org (L.-Å. Nyman).

1. Introduction

The Galactic center is one of the most extensively studied regions in our Galaxy (Oort, 1977; Brown and Liszt, 1984; Liszt, 1988; Morris and Serabyn, 1996). The inner 10 pc of our Galactic center contains several principal components: a black hole candidate, Sgr A^{*}; a spiral-shaped thermal radio source, Sgr A West; a circumnuclear disk (CND); a cluster of evolved stars; a complex of young stars; molecular and ionized gas clouds; and a powerful supernova remnant (SNR), Sgr A East (e.g., Ekers et al., 1983; Novak et al., 2000; Yusef-Zadeh et al., 2000; Schödel et al., 2003). Sgr A^{*} is thought to be surrounded by Sgr A West. The CND and Sgr A West are located in front of or just inside Sgr A East (see the review in Maeda et al., 2002), which appears to be pushing large amounts of material away from the nucleus, forming ridges of material on all sides (Pedlar et al., 1989; Mezger et al., 1989; Genzel et al., 1990; Serabyn et al., 1992; Zylka et al., 1995; McGary et al., 2001). However, some material may also move toward the nucleus, such as the NH₃ filamentary streamers, which are possibly feeding the nucleus (Okumura et al., 1989; Ho et al., 1991; Coil and Ho, 2000; McGary et al., 2001).

Neutral gas concentrated in the Galactic center is predominantly molecular and orbiting the center in the same sense as Galactic rotation (cf. Lugten et al., 1986). The molecular clouds in this region are thought to be affected strongly by the activities of the Galactic center, which produce various non-thermal and thermal features. By the interactions with these components, the molecular clouds in our Galactic center show features which are exciting but complex and difficult to interpret (e.g., Scoville, 1972; Burton and Liszt, 1978; Bally et al., 1988; Binney et al., 1991). Solomon et al. (1972) showed that most of the molecular gas very near Sgr A^{*} (within ~ 20 pc from Sgr A^{*}, in projection) is concentrated into two massive clouds, called $M - 0.02 - 0.07$ and $M - 0.13 - 0.08$, according to their Galactic coordinates (Güsten et al., 1981). $M - 0.02 - 0.07$ and $M - 0.13 - 0.08$ are also referred to as the “+50 km s⁻¹ cloud” (or sometimes the “+40 km s⁻¹ cloud”) and the “+20 km s⁻¹ cloud,” respectively. They have com-

parable masses ($\sim 5 \times 10^5 M_{\odot}$; Lis and Carlstrom, 1994) and linear dimensions (~ 10 – 15 pc), and show a complicated morphological structure (e.g., Güsten, 1989; Armstrong and Barrett, 1985; Herrnstein and Ho, 2002). The large line-widths of the observed transitions indicate that a high degree of turbulence exists.

Following the early absorption line observations of OH and H₂CO, spectral lines and dust emission from these clouds have been studied extensively (e.g., Snyder et al., 1969; Güsten and Downes, 1980; Liszt et al., 1985; Minh et al., 1992; Lis and Carlstrom, 1994), and it has been found that the physical and chemical properties of these molecular clouds differ substantially from those in the Galactic disk. The molecular properties and chemistry in the Sgr A region, however, have not been well characterized. Such characterization would provide diagnostics to understand the complicated Galactic center environment.

In this paper, we report observational results for the millimeter-wave transitions of several O-containing molecules toward the Sgr A molecular clouds, and discuss the physical and chemical properties of these clouds. Especially, we discuss the chemical gradients among the identified clouds by comparing the intensities of the observed lines, which may provide clues to understanding the complicated physical environment of our Galactic center region.

2. Observations

Observations were carried out using the 15 m Swedish-ESO telescope (SEST¹, Booth et al., 1989) on La Silla, Chile, in April 2000. We observed the ¹³CO 1–0 and 2–1, HCO⁺ 1–0, HNCO 4₀₄–3₀₃, and SiO $v = 02$ –1 transitions, using the dual channel SIS receiver which allows simultaneous observations at 3 and 1 mm. Two 1500 channel acousto-optic spectrometers with channel

¹ SEST is operated by Onsala Space Observatory, the Swedish National Facility for Radio Astronomy, with financial support from the Swedish Natural Science Research Council (NFR) and ESO.

Table 1
Line parameters of the observed spectra in Fig. 1

Molecule (transition)	V_{LSR}^a (km s $^{-1}$)	FWHM a (km s $^{-1}$)	T_A^* (K)	$\int T_A^* dv$ (km s $^{-1}$)	Rms b (K)
^{13}CO (1–0)	57.8	36.8	6.3	249.1	0.30
HCO^+ (1–0)	55.5	48.7	2.1	103.8	0.13
HNCO ($4_{04} - 3_{03}$)	53.8	23.2	1.1	27.1	0.14
SiO ($v = 02-1$)	50.7	32.7	0.6	23.8	0.17

^a Gaussian fit results.

^b R.m.s. (1σ) value of the observed spectra.

spacing of 0.69 MHz were used but the frequency resolution of the system was approximately 1.2 MHz. The HPBW and main beam efficiency are $57''$ and 0.75, respectively, at 86 GHz, and $22''$ and 0.60, respectively, at 220 GHz.

The maps were made in the region of $l = -0.2^\circ$ to $+0.3^\circ$ and $b = -0.13^\circ$ to $+0.07^\circ$ for ^{13}CO lines, and $l = -0.2^\circ$ to $+0.3^\circ$ and $b = -0.2^\circ$ to $+0.2^\circ$ for other lines, with a grid of $2'$. Spectra were taken with the position switching mode using the reference position $(l, b) = (0.0^\circ, 2.5^\circ)$. The antenna temperatures T_A^* quoted in this paper have been corrected for antenna and atmospheric losses by means of the standard chopper wheel method, but not for possible beam dilution. The typical system temperatures were about 140–180 K (SSB) in 3 mm observations, and the typical RMS of the spectra are included in Table 1.

3. Results

3.1. Observed spectra and line profiles

Fig. 1 shows sample spectra obtained near the peak position of the ^{13}CO 1–0 integrated intensity, and their line parameters are included in Table 1. The line profiles show complex velocity structures over the whole observed region, which probably result mainly from the overlap of several different velocity components in the line of sight. The ^{13}CO profiles show especially complicated structures and we first concentrate on the velocity range between 0 and 130 km s $^{-1}$.

The overall line profiles can be seen from the space–velocity map in Fig. 2, which is for the observed spectra taken along galactic longitude at $b = -0.067^\circ$. In Fig. 2, we see that the gas

clouds between $l = 0^\circ$ and 0.2° , where $M - 0.13 - 0.08$ and $M - 0.02 - 0.07$ are located, suffer a steep velocity gradient of ~ 2.5 km s $^{-1}$ pc $^{-1}$. In this figure, we can clearly see the clumpy features of the Sgr A molecular clouds. Their morphological and chemical properties will be discussed in Sections 3.2 and 4. Some spectra show high velocity wing features, as in Fig. 2(a) at $l = 0^\circ$, which extend over ± 30 km s $^{-1}$ from $V_o = 55$ km s $^{-1}$. The large FWHMs of the observed spectra suggest that there exists highly turbulent gas affected probably by the activities of

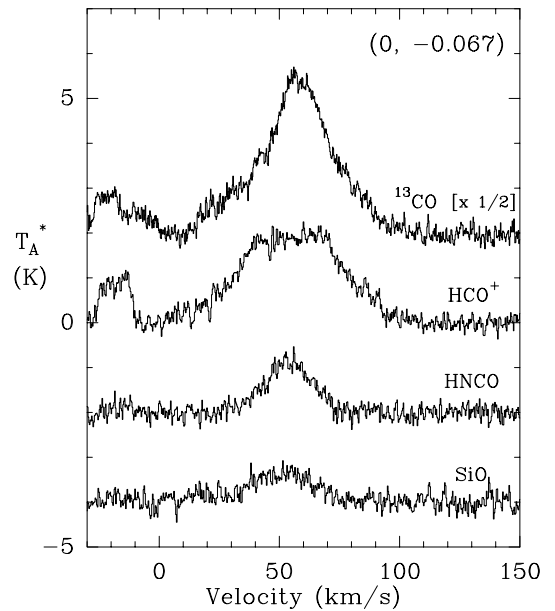


Fig. 1. Sample spectra obtained toward the position $(l, b) = (0^\circ, -0.067^\circ)$. The actual scale of the ^{13}CO 1–0 spectrum was reduced to half to fit to the indicated scale. Their line parameters are listed in Table 1.

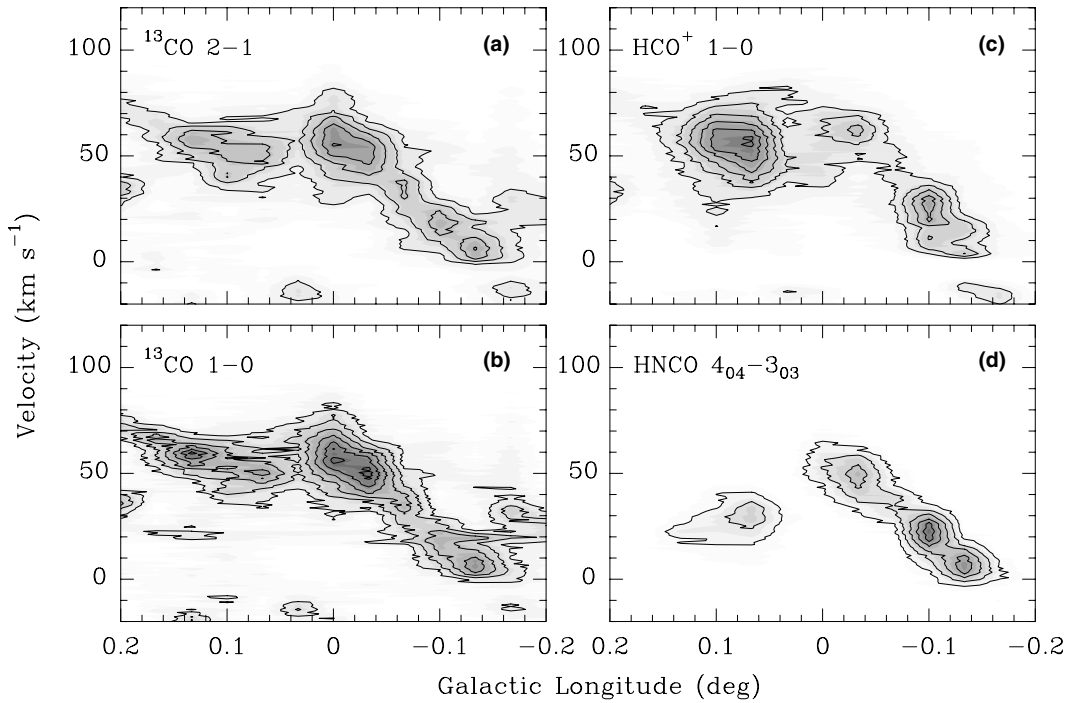


Fig. 2. Position-velocity maps taken at $b = -0.067^\circ$ along the galactic longitude of the observed region for: (a) the ^{13}CO 2–1 spectra, the contour levels increase by 1 K km s^{-1} from 1.8 K km s^{-1} , (b) ^{13}CO 1–0, contour level intervals are same as (a), (c) HCO^+ 1–0, contour levels increase by 0.6 K km s^{-1} from 1.4 K km s^{-1} , and (d) HNC0 $4_{04} - 3_{03}$, contour levels increase by 0.6 K km s^{-1} from 0.6 K km s^{-1} .

our Galactic center, in addition to large systematic motions and overlapping of different velocity components in the line of sight.

Fig. 3 shows the excitation temperatures derived using the ^{13}CO 1–0 and 2–1 lines. T_{ex} appears to be in the range of 15–20 K in the central

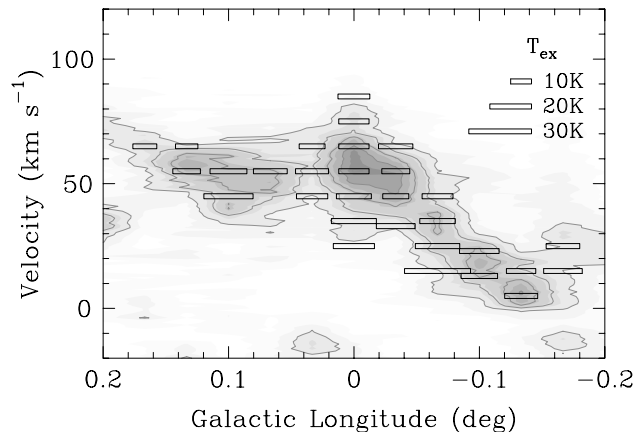


Fig. 3. Excitation temperatures derived using the ^{13}CO 1–0 and 2–1 lines at each 10 km s^{-1} interval of the spectra, overlaid on the integrated intensity map of the ^{13}CO 2–1 line. Magnitudes of the excitation temperature are indicated as the length of the bar in the upper right corner.

parts of the gas clumps, which is a typical value for general GMCs. However, T_{ex} increases to 20–30 K in the line wings and inter-clump regions. We apply $T_{\text{ex}} = 15 \pm 5$ K in deriving column densities toward locations of peak emission for the observed species other than CO.

3.2. Emission distributions

The integrated intensity maps of the observed molecules are shown in Fig. 4. Locations of the previously identified condensations are indicated as filled squares (Güsten et al., 1981). Although there must be optical depth problems, interestingly enough the observed species are enhanced at

largely different positions depending on the species, which may suggest different physical environments at the locations of the identified gas clouds.

The ^{13}CO 1–0 intensity map (see Fig. 4(a)) shows the strongest emission toward $M - 0.02 - 0.07$ (or the $+50 \text{ km s}^{-1}$ cloud). Sometimes the term $+50 \text{ km s}^{-1}$ cloud is also used to describe a larger collection of molecular gas including $M - 0.02 - 0.07$ and several other flux peaks nearby in the Galactic eastern direction. We assume that this cloud has the largest total column density among the clouds identified in Fig. 4. The abundances and clump masses have been well defined in the previous studies, but we summarize again the cloud parameters of the identified clumps in Table 3.

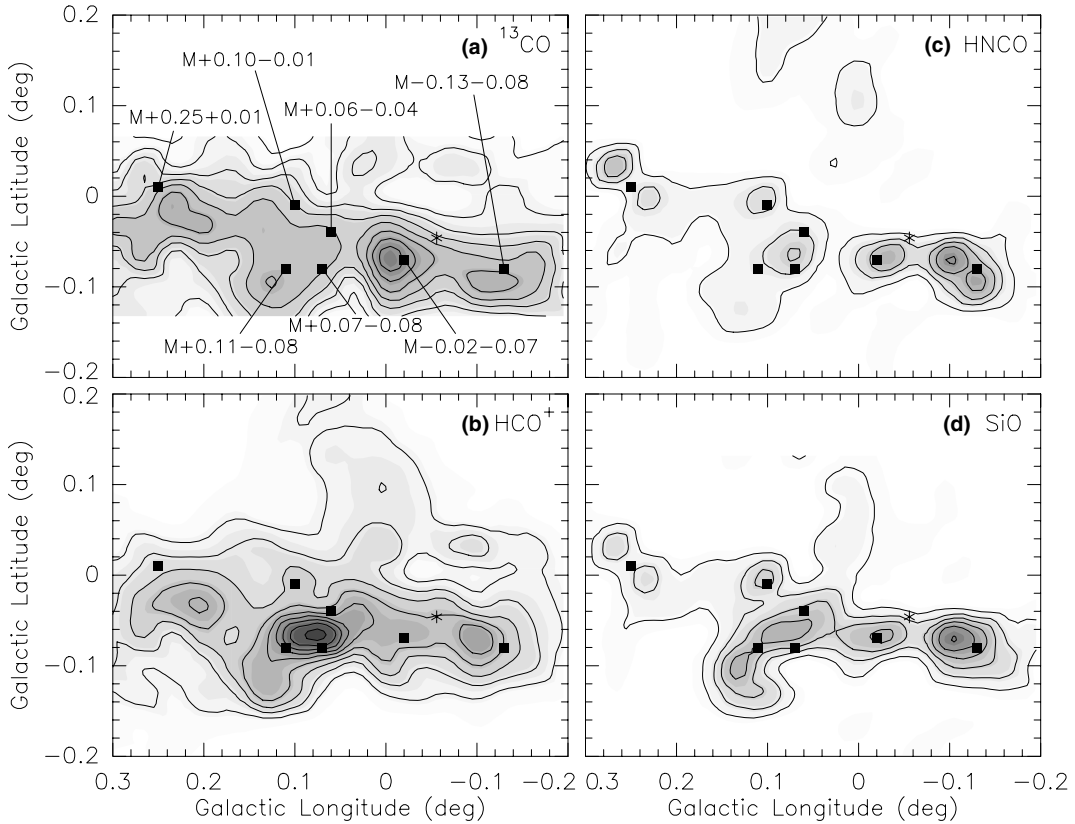


Fig. 4. Integrated intensity ($\int T_{\text{A}}^* dv$) maps of the observed lines for: (a) the ^{13}CO 1–0 transition, the contour lines increase by 30 K km s^{-1} from the lowest 25 K km s^{-1} , (b) HCO^+ 1–0, the contour increases by 20 K km s^{-1} from 30 K km s^{-1} , (c) HNCO $4_{04}-3_{03}$, the contour increases by 15 K km s^{-1} from 10 K km s^{-1} , and (d) $\text{SiO } v = 02-1$, the contour increases by 7 K km s^{-1} from 5 K km s^{-1} . The location of Sgr A* is indicated as * and the center positions of the previously identified gas condensations are indicated as filled squares.

As shown in Fig. 4(b), the HCO^+ emission appears very strong toward $M + 0.07 - 0.08$ and $M + 0.11 - 0.08$, which appear as one component with our $2'$ resolution. These two clumps could be distinguished in the previous finer spatial resolution observations (e.g., SiO 1–0 line observations: Minh et al., 2001), but they appear to share similar chemical properties in the observations for complex molecules, such as, HCO_2^+ , HNCO , and C_3H_2 (Minh et al., 1992; Lee et al., 1993). Therefore, from this HCO^+ result, we call these two clouds “the HCO^+ cloud”. The HCO^+ enhancement in this cloud may suggest that this cloud is in a different physical and chemical environment compared to other clumps in this figure.

The HNCO map in Fig. 4(c) suggests that the $M - 0.13 - 0.08$ cloud, which is known as either the +15 or +20 km s^{-1} cloud, may consist of two different components, $M - 0.13 - 0.08a$ and $M - 0.13 - 0.08b$. We can clearly separate the two components in the position-velocity map of Fig. 2(d) clearly. The representative velocities of these two components, $M - 0.13 - 0.08a$ and $M - 0.13 - 0.08b$, are $V_{\text{LSR}} = 25$ and 5 km s^{-1} , respectively.

The SiO 2–1 emission is also enhanced toward $M - 0.13 - 0.08a$ (which may be called “the +25

km s^{-1} cloud”), as shown in Fig. 4(d). Toward $M - 0.13 - 0.08b$ (“the +5 km s^{-1} cloud”), however, the SiO emission is not enhanced. The morphology and their large velocity differences may indicate that $M - 0.13 - 0.08a$ and $M - 0.13 - 0.08b$ are different clouds appearing in the same line of sight by chance. There is also strong SiO emission in the 50 km s^{-1} cloud (where ^{13}CO peaks) and the HCO^+ cloud. Martín-Pintado et al. (1997) argue that the SiO emission in the Galactic center is very fragmented and extended compared to that observed in the Galactic disk, where the SiO emission arises from much smaller regions with larger H_2 densities.

The other clouds, $M + 0.06 - 0.04$, $M + 0.10 - 0.01$, and $M + 0.25 + 0.01$, do not show distinctive features in our $2'$ resolution maps shown in Fig. 4, compared to other clouds mentioned above. We expect that finer resolution maps, especially for the HNCO or SiO transitions, are necessary to reveal the properties of these clouds.

3.3. The -30 km s^{-1} component

There is also emission at negative velocities. The spectra in Fig. 5 shows the -30 km s^{-1} emission features of the ^{13}CO 1–0 and HCO^+ 1–0 lines at

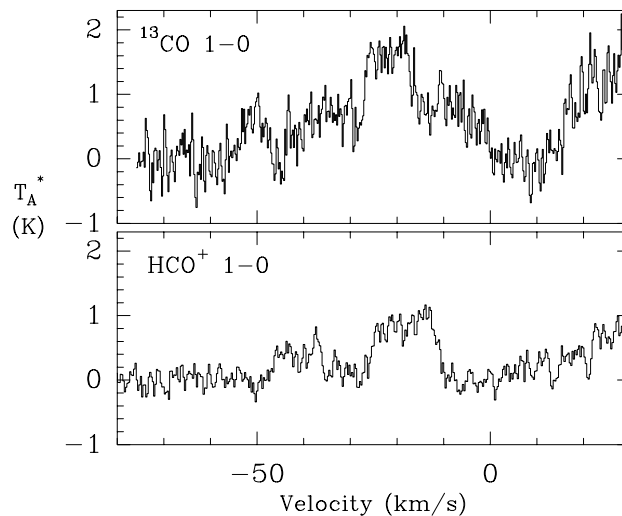


Fig. 5. ^{13}CO 1–0 and HCO^+ 1–0 spectra of the -30 km s^{-1} component obtained toward $(l,b) = (0^\circ, 0.067^\circ)$.

the position of $(l, b) = (0^\circ, 0.067^\circ)$. The HCO^+ 1–0 line clearly shows emission at different velocities, of -20 and -40 km s^{-1} , although the ^{13}CO 1–0 emission is difficult to separate into two components in this velocity range. Their line parameters are included in Table 2. The other molecules, HNCO and SiO , do not show apparent

emission features in this velocity range, which is probably a result of the smaller total column density of this component relative to other dense clouds nearby. The chemical properties of this component, however, need to be studied further.

Fig. 6 shows an integrated intensity map of the HCO^+ spectra at these two different velocities,

Table 2

Line parameters of the -30 km s^{-1} component in Fig. 5

Molecule (transition)	V_{LSR}^a (km s $^{-1}$)	FWHM a (km s $^{-1}$)	$T_{\text{A}}^*{}^a$ (K)	$\int T_{\text{A}}^* dv$ (K km s $^{-1}$)	Rms b (K)
^{13}CO (1–0)	-21.2	27.5	1.4	42.4	0.30
HCO^+ (1–0)	-17.9	12.5	1.0	12.8	0.14
	-40.3	10.9	0.5	5.5	0.14

^a Gaussian fit results.

^b R.m.s. (1σ) value of the observed spectra.

Table 3

Cloud parameters identified in the observed region

Cloud name	Included clump	Size a (pc)	$N(\text{H}_2)^b$ (cm $^{-2}$)	Mass c (M_{\odot})
+50 km s $^{-1}$ cloud	$M - 0.02 - 0.07$	13	9×10^{22}	3×10^5
The HCO^+ cloud	$M + 0.07 - 0.08$ $M + 0.11 - 0.08$	15	6×10^{22}	2×10^5
+25 km s $^{-1}$ cloud	$M - 0.13 - 0.08a$	10	5×10^{22}	9×10^4
+5 km s $^{-1}$ cloud	$M - 0.13 - 0.08b$	8	5×10^{22}	6×10^4

^a Average of long and short axes from Fig. 12.

^b Using ^{13}CO 1–0, assuming optically thin emission, $T_{\text{rot}} = 15 \text{ K}$ (cf. Sections 3.1 and 4) and the abundance ratio $\text{H}_2/^{13}\text{CO} = 2.5 \times 10^5$ (Section 3.3).

^c Using $N_{\text{tot}}(\text{H}_2) \times 2 \times \mu_{\text{H}} \times \text{Area}$, where $\mu = 1.36 \text{ amu}$ per H nuclei accounts for the mass of He and other elements.

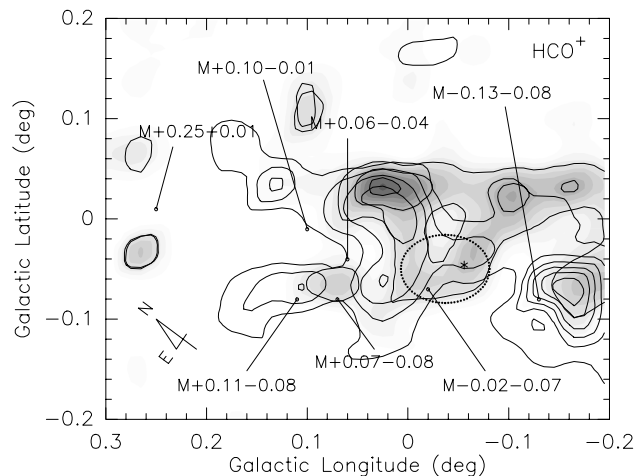


Fig. 6. The integrated intensity map of the HCO^+ 1–0 line for the velocity range between -30 and 0 km s^{-1} (thick lines) and -60 and -30 km s^{-1} (dashed lines and grey scale). Both contours increase by 4 K km s^{-1} from the lowest 4 K km s^{-1} . The dotted ellipse around Sgr A* indicates a rough position of Sgr A East.

–20 and –40 km s^{–1}. The –20 km s^{–1} component shows stronger features than the –40 km s^{–1} component, but they show similar distributions and, for convenience, we call these two velocity components together “the –30 km s^{–1} cloud”. This cloud appears to be located near and to the north of Sgr A East, and its morphology seems to indicate that it lies between Sgr A East and the known gas clumps to the east side of Sgr A East. The maps of this velocity component for the ¹³CO 1–0 and 2–1 lines show very similar features to those of HCO⁺ 1–0 in Fig. 6.

We derive the total ¹³CO column density (N_{tot}) toward the peak emission position (l, b) = (0.033°, 0.033°) to be $N_{\text{tot}}(^{13}\text{CO}) = (2.0 \pm 0.4) \times 10^{17} \text{ cm}^{-2}$, assuming optically thin emission and the value $T_{\text{ex}} = 15\text{--}25 \text{ K}$ derived for this component by comparing the ¹³CO 1–0 and 2–1 lines. The size of this component is $\sim 17 \text{ pc} \times 11 \text{ pc}$ (long axis \times short axis) from the HPW size of the ¹³CO emission region. To estimate the total mass of this component, we use the conversion ratio $\text{H}_2/^{13}\text{CO} = 2.5 \times 10^5$ from the values $\text{CO}/\text{H}_2 = 10^{-4}$ and $\text{CO}/^{13}\text{CO} \approx 25$ for our Galactic center region (cf.

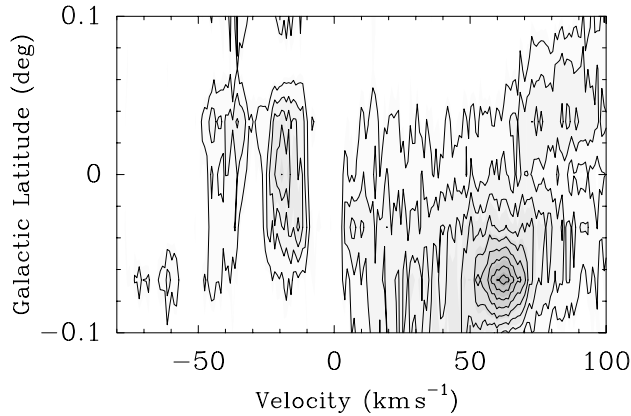


Fig. 7. Position-velocity map of the HCO⁺ 1–0 line obtained at the selected positions: (l, b [deg])=(0.10, 0.10), (0.07, 0.07), (0.03, 0.03), (0, 0), (0, –0.03), (–0.03, –0.07), and (–0.07, –0.10). The contour levels increase by 0.3 K from the lowest contour of 0.2 K.

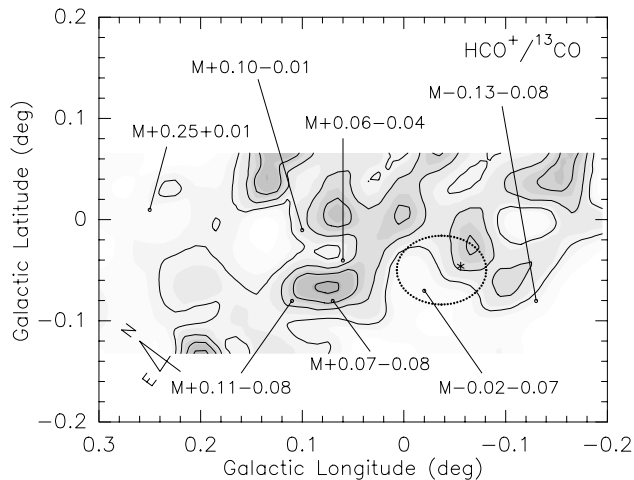


Fig. 8. Integrated intensity ratio of the observed HCO⁺ 1–0 and ¹³CO 1–0 lines. The contour levels increase by 0.2 from 0.6.

Minh et al., 1992). The derived total mass of this component is $\sim 1.7 \times 10^5 M_{\odot}$.

In Fig. 7, we show the position-velocity map obtained along a cut through the peak of this component. This -30 km s^{-1} component appears to be well isolated from the ‘main’ emission near $V_{\text{LSR}} = 60 \text{ km s}^{-1}$. The spectral features and morphology suggest that this former component is isolated and probably associated with and affected by Sgr A East. But it is not certain whether the large velocity difference with respect to the ‘main’ emission actually indicates a substantial relative motion with respect to the general body of gas in the region or an unrelated, separated cloud, although its morphology gives the appearance of association with other features near the Galactic center region. The shape of this component also looks very similar to that of the region showing relative enhancement of the HCO^+ ‘main’ emission in Fig. 8. This component needs further investigation to reveal its actual association with Sgr A East and the surrounding gas clumps.

4. Discussion

We see apparent differences in the emission morphologies of the observed molecular species, as shown in Fig. 4. This is certainly telling us that there exist chemical differences among the different cloud components, which presumably have mainly resulted from the different physical environments at different locations. To see the chemical gradients clearly, we shall plot the relative intensities of the observed transitions.

In Fig. 8, we show the map of the observed intensity ratio of the HCO^+ 1–0 and the ^{13}CO 1–0 intensities. If we assume that ^{13}CO generally traces the total column density, this ratio may reveal specific features related to HCO^+ chemistry. HCO^+ appears to be enhanced relative to ^{13}CO toward the northeast direction from Sgr A East in the region $l = 0.1^\circ - 0^\circ$, and shows the largest enhancement toward $M + 0.07 - 0.08$ and $M + 0.11 - 0.08$ (the HCO^+ cloud). Overall, the HCO^+ enhanced region seems to be connected as one continuous component, and may be located close to Sgr A East, which is a dominant radio feature of our

Galactic center (Downes and Martin, 1971; Yusef-Zadeh and Morris, 1987). Lee et al. (2003) observed the vibrationally excited H_2 emission lines and argue that Sgr A East shocks the ambient molecular clouds. Sgr A East, an expanding SNR, is known to shock nearby gas clumps as observed with the vibrationally excited H_2 lines (e.g., Lee et al., 2003).

It has been known that there are significant changes in the abundance ratio of HCO^+/CO depending on the total column density. In the typical dark clouds the abundance ratio of HCO^+/CO appears to be about 4×10^{-3} , but increases toward the diffuse cloud region by a factor of up to 10 (Guélin et al., 1982; Lucas and Liszt, 1994). HCO^+ is formed at a more primitive level of the chemistry than other complex species and is closely linked with CO. Turner (1995) argues that, in dense clouds, essentially all free carbon is in the form of CO, and HCO^+ is formed by the reaction between H_3^+ and CO, but in diffuse clouds, both HCO^+ and CO are formed by the reaction between C^+ and OH, while CO is destroyed primarily by photodissociation.

Although the optical depths of the observed lines are expected to be large ($\tau \gg 1$: Minh et al., 1992), we applied the optically thin line assumption to compare the relative abundances and distributions of the molecules to roughly estimate the chemical gradients over relatively large scales. We then calculate total column densities of HCO^+ and ^{13}CO toward the $(l, b) = (0^\circ, -0.067^\circ)$ position, for example, to be $N_{\text{tot}}(\text{HCO}^+) = (1.3 \pm 0.3) \times 10^{14} \text{ cm}^{-2}$ and $N_{\text{tot}}(^{13}\text{CO}) = (3.7 \pm 0.7) \times 10^{17} \text{ cm}^{-2}$, assuming the excitation temperature, $T_{\text{ex}} = 15 \pm 5 \text{ K}$ (Section 3.1). The error ranges are calculated solely from the rotation temperature range applied, since the signal-to-noise ratio of the spectra is very large, as included in Table 1.

These column densities give an HCO^+/CO abundance ratio of 3.5×10^{-4} , with an error of $\sim 5\%$ of the value, considering only the uncertainty in T_{ex} . One can multiply 8.2×10^{-4} by the contour levels in Fig. 8 to find the abundance ratio at any position on the map, under the same assumptions. Toward the column density peak, $M - 0.02 - 0.07$ ($+50 \text{ km s}^{-1}$ cloud), we derive the HCO^+ and ^{13}CO abundance ratio, to be about $\sim 4 \times 10^{-4}$. Near the HCO^+ peak emission positions of $M + 0.07 - 0.08$

(the HCO^+ cloud) and the inter-cloud region where HCO^+ is enhanced ($l = 0.1^\circ - 0^\circ$; Fig. 8), the abundance ratios of $\text{HCO}^+/\text{}^{13}\text{CO}$ appear to be $\sim 1 \times 10^{-3}$, a factor of 2–3 larger than at other regions in the observed area. These values are less than those for the Galactic plane clouds by more than a factor of a few (Turner, 1995). Further studies of the possible effects of the optical depth and isotopic abundance variations for the observed species are needed to reliably compare the values with those of Galactic plane clouds. In fact, HC^{18}O^+ observations suggest that we may have underestimated the HCO^+ abundance in this region (Minh et al., 1992).

Irrespective of the absolute abundance ratio, however, HCO^+ appears to be enhanced toward the “ HCO^+ cloud” and the “inter-cloud” region in Fig. 8, relative to other clouds identified in the observed area. We think that the “diffuse chemistry” for HCO^+ may work more effectively in the HCO^+ enhanced region, increasing the abundance ratio by a factor of 2–3 compared with the other clumps in the observed area. Recently, Rawlings et al. (2004) argue that shocks from the outflow jets enhance the HCO^+ abundance by the interaction with the surrounding envelope, as a result of shock-induced desorption and photoprocessing of dust grain ice mantles. As shown in Fig. 9, there exist a lot of complex thermal and nonthermal features in the HCO^+ enhanced region in Fig. 8,

suggesting that shocks and high-energy photons will play significant roles in characterizing this region (Figer et al., 2002; Yusef-Zadeh, 2003). Therefore, we may argue that the HCO^+ enhanced region is located closer to Sgr A East than other gas clumps identified in the observed area.

The 50 km s^{-1} cloud ($M - 0.02 - 0.07$) does not show any relative enhancement in the observed HCO^+ , HNCO , and SiO emission features, but appears to show the largest ^{13}CO column density. This cloud appears to be relatively chemically quiescent in our observations, which may suggest that it is located farther from the active Galactic center than other identified clouds in this region. The curved molecular ridge, which is considered to be a portion of the 50 km s^{-1} cloud compressed by the expanding Sgr A East, is thought to lie just outside Sgr A East (Ho et al., 1985; Genzel et al., 1990; Serabyn et al., 1992). If we argue that this 50 km s^{-1} cloud is chemically quiescent, then this curved ridge may be formed as a result of the interaction of the Sgr A East SNR with the HCO^+ cloud ($M + 0.07 - 0.08$), probably not with the 50 km s^{-1} cloud ($M - 0.02 - 0.07$). Then, this ridge is located “behind” the $+50 \text{ km s}^{-1}$ cloud, if the 50 km s^{-1} cloud is assumed to be located closer to us than other clouds in this region.

In Fig. 10, we show a map similar to Fig. 8, but for the observed $\text{HNCO}/^{13}\text{CO}$ ratio. The $\text{HNCO}/^{13}\text{CO}$ emission ratio appears to be

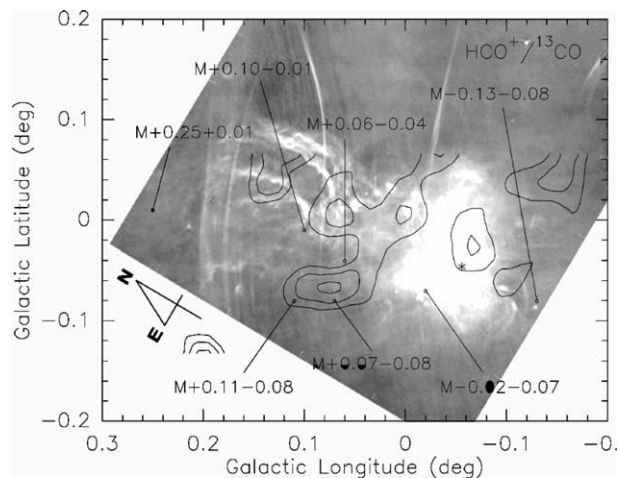


Fig. 9. Overlap of the radio continuum map (Lang et al., 1999) and the HCO^+ 1–0 and ^{13}CO 1–0 intensity ratio map of Fig. 8.

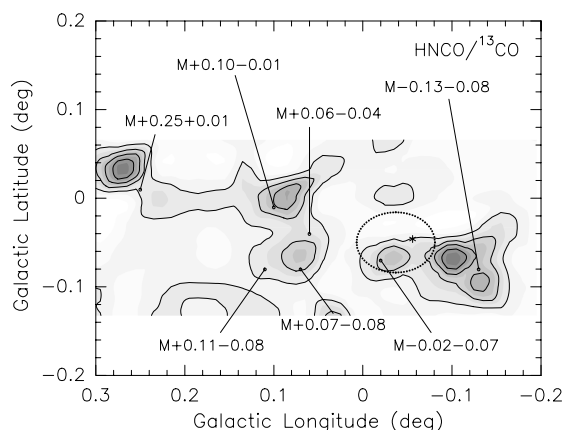


Fig. 10. Integrated intensity ratio between the observed HNC0 $4_{04}-3_{03}$ and ^{13}CO 1–0 lines. The contour levels increase by 0.1 from 0.1. This contour level times 1.1×10^{-2} gives the abundance ratio if the same assumptions as for the HCO^+/CO abundance ratio calculation in this section are applied.

enhanced toward $M - 0.13 - 0.08a$ and also toward $M + 0.25 + 0.01$. The previous observations of HNC0 toward Sgr B2 (Minh et al., 1998) have shown very interesting features: the peak positions and velocity properties are certainly different from those of other molecular transitions detected in this region. We think that the formation of HNC0 may be related to the effect on interstellar grain ice mantles of Galactic center activities. The HCO_2^+

molecule, which is a slightly asymmetric molecule like HNC0, shows very similar features with HNC0 towards Sgr B2. HCO_2^+ is thought to be a precursor of gas phase CO_2 and is observed only toward our Galactic center, possibly as a result of the effects on interstellar grain ice mantles of some kinematical activities (Minh et al., 1998, 1988). It has been found that there exist “streamers” reaching out from $M - 0.13 - 0.08a$ toward Sgr A East, which seems to be feeding into the CND (Okumura et al., 1991; Ho et al., 1991; Coil and Ho, 2000). Although the relative locations of $M - 0.13 - 0.08$ and Sgr A East are still controversial (McGary et al., 2001; Lee et al., 2003), the prominent HNC0 feature toward $M - 0.13 - 0.08a$ may be related with the kinematical association or interaction of this cloud with Sgr A East. We assume that this cloud is located very close to Sgr A East, so that the HNC0 and SiO emissions are enhanced by the interaction with Sgr A East. There is little previous research on the other “HNC0 clump”, $M + 0.25 + 0.01$, and further studies on this cloud may show interesting connections with the clouds near Sgr A East.

The $\text{SiO}/^{13}\text{CO}$ ratio is shown in Fig. 11. SiO has been considered a high-temperature tracer, since most Si has been thought to be locked up in grains in quiet regions, and can return to the gas phase

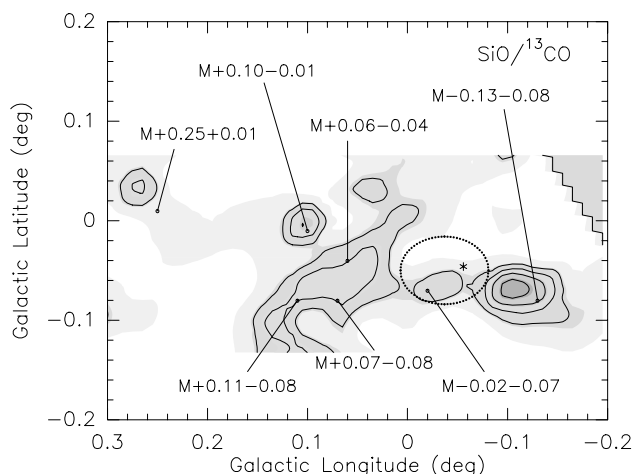


Fig. 11. Integrated intensity ratio between the observed lines for SiO 2–1 and ^{13}CO 1–0. The contour levels increase by 0.05 from 0.1. This contour level times 2.0×10^{-3} gives the abundance ratio if the same assumptions as for the HCO^+/CO abundance ratio calculation in this section are applied.

only by the effects of high-energy photons or shocks (Downes et al., 1982; Ziurys and Friberg, 1987; Langer and Glassgold, 1990). While SiO gives rise to prominent maser lines toward late-type stars and a limited class of star forming regions, the thermal emission of this molecule is, in general, very weak except in the Galactic center clouds. Consequently, the enhancement of SiO thermal emission may also indicate that shocks and high energy photons are prevalent in the Galactic center region. The SiO emission appears to be enhanced strongly toward the 25 km s^{-1} cloud ($M - 0.13 - 0.08a$) which again indicates that this region may be interacting directly with Sgr A East.

A possible enhancement of SiO toward the HCO^+ enhanced inter-cloud region also suggests that this region is affected by large-scale fast shocks from Sgr A East. Since SiO is thought of as an unambiguous tracer of high temperature and/or shock chemistry in interstellar clouds (Martí-Pintado et al., 1997), further studies on SiO are desirable to reveal the large-scale properties of the interacting regions in the Galactic center.

5. Conclusions

We observed millimeter-wave molecular lines of CO, HCO^+ , HNC, and SiO toward the Sgr

A region using the SEST telescope at LaSilla, Chile. The comparison of the observed transitions shows that the several prominent gas condensations in this region have very distinctive chemical properties with respect to each other, which may result from the different physical conditions at different locations. Fig. 12 shows a schematic diagram of the components re-identified in these observations and Table 3 summarizes their cloud parameters.

Our HNC and SiO observations suggest that $M - 0.13 - 0.08$, which is known as the $+20 \text{ km s}^{-1}$ cloud, seems to consist of two different components, $M - 0.13 - 0.08a$ and $M - 0.13 - 0.08b$, with LSR velocities of about 25 and 5 km s^{-1} , respectively. The $M - 0.13 - 0.08a$ clump (the 25 km s^{-1} cloud) seems to be located very close to Sgr A East, and the enhancement of HNC and SiO may be a result of the direct interaction with this SNR. The $M - 0.13 - 0.08b$ clump (the 5 km s^{-1} cloud) may be separated and only appear to be connected because it is on the line of sight to the $M - 0.13 - 0.08a$ clump.

The molecular gas clump $M - 0.02 - 0.07$ (the $+50 \text{ km s}^{-1}$ cloud) shows the strongest ^{13}CO emission, which indicates that this cloud has the largest column density and is the most massive condensation among the cloud components shown in Fig. 12. We estimate that its mass is $\geq 3 \times 10^5 M_{\odot}$. It may be located farther from

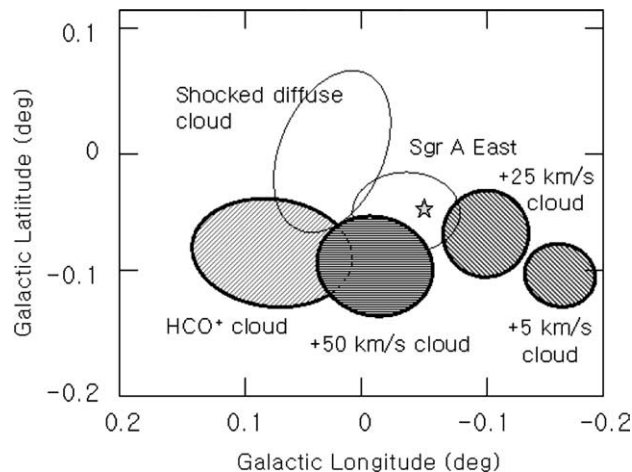


Fig. 12. Schematic diagram of the molecular clouds re-identified in this observation.

Sgr A* and closer to us than other clouds around, since it appears to be chemically more quiescent than other clouds in Fig. 12 and seems to shade the inter-cloud region where the $\text{HCO}^+/\text{}^{13}\text{CO}$ ratio is enhanced. The -30 km s^{-1} component, observed in the HCO^+ and ^{13}CO spectra, shows a similar morphology to the HCO^+ enhanced “inter-cloud” region. This velocity component seems to be associated with the Sgr A East neutral gas region, but its nature needs to be studied further.

$M + 0.07 - 0.08$ and $M + 0.11 - 0.08$ seem to share similar chemical properties and they appear to be one cloud in our observations. These clumps show the strongest $\text{HCO}^+ 1-0$ emission among the identified clouds in Fig. 12, and may be called “the HCO^+ cloud”. The $\text{HCO}^+/\text{}^{13}\text{CO}$ abundance ratio is enhanced by a factor of 2–3 toward the HCO^+ cloud and the inter-cloud region between $l = 0.1^\circ$ and 0° right near Sgr A East. This inter-cloud region may be an extended component of the HCO^+ cloud ($M + 0.07 - 0.08$ and $M + 0.11 - 0.08$). The relative enhancement of HCO^+ is thought to result from shocks produced by interaction with Sgr A East. The HCO^+ chemistry clearly needs further study.

Acknowledgments

S.J.K. and Y.C.M. acknowledge a partial support from KOSEF (R01-1999-000-00022-0), and W.I. from the NASA Astrobiology Institute through the Goddard Space Flight Center node.

References

- Armstrong, J.T., Barrett, A.H., 1985. *ApJS* 57, 535.
- Bally, J., Stark, A.A., Wilson, R.W., Henkel, C., 1988. *ApJ* 324, 223.
- Binney, J., Gerhard, O.E., Stark, A.A., Bally, J., Uchida, K.I., 1991. *MNRAS* 525, 210.
- Booth, R.S., Delgado, G., Hagsrom, M., Johansson, L.E.B., Murphy, D.C., 1989. *A&A* 216, 315.
- Brown, R.L., Liszt, H.S., 1984. *ARAA* 22, 223.
- Burton, W.B., Liszt, H.S., 1978. *ApJ* 225, 815.
- Coil, A.L., Ho, P.T.P., 2000. *ApJ* 533, 245.
- Downes, D., Genzel, R., Hjalmarson, A., Nyman, L.A., Ronnang, B., 1982. *ApJ* 252, L29.
- Downes, D., Martin, A.H.M., 1971. *Nature* 233, 112.
- Ekers, R.D., van Gorkom, J.H., Schwarz, U.J., Goss, W.M., 1983. *A&A* 122, 143.
- Figer, D.F., et al., 2002. *ApJ* 581, 258.
- Genzel, R., Stacey, G.J., Harris, A.I., Townes, C.H., Geis, N., Graf, U.U., Poglitsch, A., Stutzki, J., 1990. *ApJ* 356, 160.
- Güsten, R., 1989. In: Morris, M. (Ed.), *IAU Symposium*, vol. 136. Kluwer, Dordrecht. p. 89.
- Güsten, R., Downes, D., 1980. *A&A* 87, 6.
- Güsten, R., Walmsley, C.M., Pauls, T., 1981. *A&A* 103, 197.
- Guélin, M., Langer, W.D., Wilson, R.W., 1982. *A&A* 107, 107.
- Herrnstein, R.M., Ho, P.T.P., 2002. *ApJ* 579, L83.
- Ho, P.T.P., Ho, L.C., Szczepanski, J.C., Jackson, J.M., Armstrong, J.T., Barrett, A.H., 1991. *Nature* 350, 309.
- Ho, P.T.P., Jackson, J.M., Barrett, A.H., Armstrong, J.T., 1985. *ApJ* 288, 575.
- Lang, C.C., Morris, M., Echevarria, L., 1999. *ApJ* 526, 727.
- Langer, W.D., Glassgold, A.E., 1990. *ApJ* 352, 121.
- Lee, C.W., Minh, Y.C., Irvine, W.M., 1993. *J.K.A.S.* 26, 69.
- Lee, S., Pak, S., Davis, C.J., Herrnstein, R.M., Geballe, T.R., Ho, P.T.P., Wheeler, J.C., 2003. *MNRAS* 341, 509.
- Lis, D.C., Carlstrom, J.E., 1994. *ApJ* 424, 189.
- Liszt, 1988. In: Verschuur, G.L., Kellermann, K.I. (Eds.), *Galactic and Extragalactic Radio Astronomy*. Springer-Verlag, New York, p. 359.
- Liszt, H.S., Burton, W.B., van der Hulst, J.M., 1985. *A&A*, 142, 237.
- Lucas, Liszt, 1994. *A&A* 282, L5.
- Lugten, J.B., Genzel, R., Crawford, M.K., Townes, C.H., 1986. *ApJ* 306, 691.
- Maeda, Y., et al., 2002. *ApJ* 570, 671.
- Martin-Pintado, J., De Vicente, P., Fuente, A., Planesas, P., 1997. *ApJ* 482, L45.
- McGary, R.S., Coil, A.L., Ho, P.T.P., 2001. *ApJ* 559, 326.
- Mezger, P.G., Zylka, R., Salter, C.J., Wink, J.E., Chini, R., Kreysa, E., Tuffs, R., 1989. *A&A* 209, 337.
- Minh, Y.C., Haikala, L., Hjalmarson, Å., Irvine, W.M., 1998. *ApJ* 498, 261.
- Minh, Y.C., Irvine, W.M., Friberg, P., 1992. *A&A* 258, 489.
- Minh, Y.C., Irvine, W.M., Ziurys, L.M., 1988. *ApJ* 334, 175.
- Minh, Y.C., Roh, D.-G., Kim, S.-J., Ohishi, M., 2001. *Publ.K.A.S.* 16, 5.
- Morris, M., Serabyn, E., 1996. *ARAA* 34, 645.
- Novak, G., Dotson, J.L., Dowell, C.L., Hildebrand, R.H., Renbarger, T., Schleuning, D.A., 2000. *ApJ* 529, 241.
- Okumura, S.K., et al., 1989. *ApJ* 347, 240.
- Okumura, S.K., Ishiguro, M., Fomalont, E.B., Hasegawa, T., Kasuga, T., Morita, K.-I., Kawabe, R., Kobayashi, H., 1991. *ApJ* 378, 127.
- Oort, J., 1977. *ARAA* 15, 295.
- Pedlar, A., et al., 1989. *ApJ* 342, 769.
- Rawlings, J.M.C., Redman, M.P., Keto, E., Williams, D.A., 2004. *MNRAS* 351, 1054.
- Schödel, R., Ott, T., Genzel, R., Eckart, A., Mouawad, N., Alexander, T., 2003. *ApJ* 596, 1015.
- Scoville, N.Z., 1972. *ApJ* 175, L127.

- Serabyn, E., Lacy, J.H., Achterman, J.M., 1992. *ApJ* 395, 166.
- Snyder, L.E., Zuckerman, B., Buhl, D., Palmer, P., 1969. *BAAS* 1, 363.
- Solomon, P.M., Scoville, N.Z., Jefferts, K.B., Penzias, A.A., Wilson, R.W., 1972. *ApJ* 178, 125.
- Turner, B.E., 1995. *ApJ* 449, 635.
- Yusef-Zadeh, F., 2003. *ApJ* 598, 325.
- Yusef-Zadeh, F., Morris, M., 1987. *ApJ* 320, 545.
- Yusef-Zadeh, F., Melia, F., Wardle, M., 2000. *Science* 287, 85.
- Ziurys, L.M., Friberg, P., 1987. *ApJ* 314, L49.
- Zylka, R., Mezger, P.G., Ward-Thompson, D., Duschl, W.J., Lesch, H., 1995. *A&A* 297, 83.